

## Exposing hypersensitivity in quantum chaotic dynamics

Andrzej Grudka <sup>1</sup>, Paweł Kurzyński <sup>1,\*</sup>, Adam S. Sajna,<sup>2</sup> Jan Wójcik <sup>3</sup> and Antoni Wójcik <sup>1</sup>

<sup>1</sup>*Institute of Spintronics and Quantum Information, Faculty of Physics, Adam Mickiewicz University, 61-614 Poznań, Poland*

<sup>2</sup>*Institute of Theoretical Physics, Faculty of Fundamental Problems of Technology, Wrocław University of Science and Technology, 50-370 Wrocław, Poland*

<sup>3</sup>*Faculty of Physics, Adam Mickiewicz University, 61-614 Poznań, Poland*



(Received 4 August 2023; accepted 27 November 2023; published 21 December 2023)

We study hypersensitivity to initial-state perturbation in the unitary dynamics of a multiqubit system. We use the quantum state metric, introduced by Girolami and Anza [*Phys. Rev. Lett.* **126**, 170502 (2021)], which can be interpreted as a quantum Hamming distance. To provide a proof of principle, we take the multiqubit implementation of the quantum kicked top, a paradigmatic system known to exhibit quantum chaotic behavior. Our findings confirm that the observed hypersensitivity corresponds to commonly used signatures of quantum chaos. Furthermore, we demonstrate that the proposed metric can detect quantum chaos in the same regime and under analogous initial conditions as in the corresponding classical case.

DOI: [10.1103/PhysRevE.108.064212](https://doi.org/10.1103/PhysRevE.108.064212)

### I. INTRODUCTION

Hypersensitivity to small perturbations is a defining characteristic of classical chaos [1]. On the other hand, it is usually assumed that there is no state sensitivity in the quantum realm [2–4], although it can emerge in the correspondence limit [5], in particular under decoherence [6]. To deal with this problem different methods to detect chaotic behavior in the quantum domain were proposed. Instead of state sensitivity, one can observe sensitivity to Hamiltonian perturbation [4] which can be measured, e.g., by the Loschmidt echo [7–9]. A related concept to the Loschmidt echo is known as the out-of-time-order correlator (OTOC) [10–13]. Also, commonly used methods to detect quantum chaos consist of examining the statistics of energy levels and eigenstates [14–17]. Finally, it is also worth mentioning entanglement dynamics as yet another powerful tool to investigate this problem [18–21].

In this paper we study the detection of quantum chaos using the primordial concept of quickly growing distance between the original and the perturbed state. We stress that not every quantum state metric is suitable for this task. The problem of finding a proper metric comes from three facts. First, quantum states are not represented as points in phase space, but as vectors in Hilbert space. Second, a scalar product (overlap) between quantum states is invariant under unitary dynamics and consequently, no sensitivity to perturbation can be detected through any metric based on it. Finally, some quantum state metrics can be naturally used as a measure of how well two states can be distinguished. However, even perfectly distinguishable states, yielding the same maximal distance, can differ in a physically meaningful way. These issues were already noticed in Ref. [22], where the physical distance, based on the Wasserstein distance, was introduced. We note that

the Wasserstein distance has already found applications as a quantum state metric [23–26]. The physical distance of Ref. [22] is basis dependent, i.e., it is a distance between probability distributions on a metric space. The choice of the measurement basis and the underlying metric on the set of basis states depends on the physical property in which one is interested. The authors of Ref. [22] used the physical distance to derive quantum Lyapunov exponents and to evaluate their classical limits. Moreover, they used it as a measure of quantum chaos for three models: quantum kicked rotor, three-site Bose-Hubbard model, and a spin chain.

Here, we use a basis-independent distance that is a slight modification of the metric proposed by Girolami and Anza [27] which can be called quantum Hamming distance (QHD). We apply QHD to the multiqubit implementation of the quantum kicked top. We choose it because QHD is extremely well adjusted to systems living in Hilbert space possessing natural tensor product structure. In addition, the kicked top is a very well-known system [2,9,18–20,28–43] and our goal is not so much to study its behavior as to prove that divergence of states in Hilbert space, as measured by QHD, can provide a reliable description of chaotic dynamics.

### II. QUANTUM HAMMING DISTANCES

Let us emphasize that the need for no overlap-based metric is not limited to the field of quantum chaos. An important concern regarding the overlap metric is its inability to detect differences between states that are physically significant [22]. Let us consider as an example three states of  $n$  qubits,

$$|\psi_1\rangle = |000 \dots 00\rangle, \quad (1)$$

$$|\psi_2\rangle = |000 \dots 01\rangle, \quad (2)$$

$$|\psi_3\rangle = |111 \dots 11\rangle. \quad (3)$$

\*pawel.kurzynski@amu.edu.pl

Due to their mutual orthogonality, the overlap metric yields  $\text{dist}(\psi_1, \psi_2) = \text{dist}(\psi_1, \psi_3) = \text{dist}(\psi_2, \psi_3)$ . However, the states  $|\psi_1\rangle$  and  $|\psi_2\rangle$  bare a much more physical resemblance than  $|\psi_1\rangle$  and  $|\psi_3\rangle$ , or  $|\psi_2\rangle$  and  $|\psi_3\rangle$ . In particular, an initial microscopic perturbation

$$|\psi_1\rangle \rightarrow |\delta_1\rangle = \sqrt{1-\delta}|\psi_1\rangle + \sqrt{\delta}|\psi_2\rangle \quad (4)$$

can unitarily evolve into a macroscopically different state

$$|\delta_2\rangle = \sqrt{1-\delta}|\psi_1\rangle + \sqrt{\delta}|\psi_3\rangle. \quad (5)$$

The overlap metric fails to capture the aforementioned micro-macro differences, which can be crucial in quantum chaotic systems. Put simply, the overlap metric quantifies how well two quantum states can be distinguished, and in the case of states (1)–(3), they are perfectly distinguishable. However, many important properties of these states extend far beyond mere distinguishability.

Let us consider quantum state metrics that can be interpreted as QHDs. The fundamental idea behind QHD (given by Girolami and Anza [27]) involves a partition, denoted as  $P$ , which divides the system into parts labeled as  $a = 1, 2, \dots, a_{\max}$  ( $1 \leq a_{\max} \leq n$ ). Each part contains  $k_a$  elements, hence  $\sum_{a=1}^{a_{\max}} k_a = n$ . Let  $\rho$  and  $\sigma$  represent two states of an  $n$ -partite system. The QHD between  $\rho$  and  $\sigma$  is defined [27] as

$$D(\rho, \sigma) = \max_P \delta_P(\rho, \sigma), \quad (6)$$

$$\delta_P(\rho, \sigma) = \sum_a \frac{1}{k_a} d(\rho_a, \sigma_a), \quad (7)$$

where  $\rho_a$  and  $\sigma_a$  are the states of subsystems with respect to a given partition  $P$ . In the above  $d(\dots)$  is a metric which we will discuss in a moment. The definition of the QHD, specifically Eq. (7), relies on the additivity. In particular, the additivity means that  $D(\rho \otimes \tilde{\rho}, \sigma \otimes \tilde{\sigma}) = D(\rho, \sigma) + D(\tilde{\rho}, \tilde{\sigma})$ . In addition, note that  $\delta_P(\rho, \sigma)$  is not a metric. This is because for some partition  $P$  two different states  $\rho \neq \sigma$  may give rise to  $\rho_a = \sigma_a$  for all  $a$ , which implies  $\delta_P(\rho, \sigma) = 0$ . But the metric should be equal to zero if and only if  $\rho = \sigma$ . This is the reason why maximization is used in the definition (6).

In the original version, Girolami and Anza [27] use a Bures length (also known as a Bures angle) [44]

$$d(\rho, \sigma) = \cos^{-1}(\text{Tr}\sqrt{\sigma^{1/2}\rho\sigma^{1/2}}). \quad (8)$$

However, in the subsequent sections of this paper, we employ the distance metric based on trace distance [44,45]

$$d(\rho, \sigma) = \frac{1}{2} \text{Tr}|\rho - \sigma|. \quad (9)$$

The choice of using the trace distance is motivated by its numerical tractability, as it is generally easier to evaluate computationally (especially when two states are almost identical) compared to the Bures length. The additivity property of the QHD based on trace distance is proven in Appendix A. With this choice, one obtains for our exemplary states (1)–(3)

$$D(\psi_1, \psi_2) = 1, \quad (10)$$

$$D(\psi_1, \psi_3) = n, \quad (11)$$

and

$$D(\psi_2, \psi_3) = n - 1. \quad (12)$$

This is why we called this metric QHD. At this point it is worth mentioning that the classical Hamming distance can be also used to study properties of complex quantum systems [46].

Additionally, to streamline our analysis, we note that for any partition  $P$ , QHD is lower bounded by  $\delta_P(\rho, \sigma)$ ,

$$\delta_P(\rho, \sigma) \leq D(\rho, \sigma). \quad (13)$$

Therefore, if  $\delta_P(\rho, \sigma)$  is hypersensitive to perturbation, then so is  $D(\rho, \sigma)$ .

Recently, one of us demonstrated in Ref. [47] that the QHD can detect state sensitivity in specific quantum dynamics involving three-body interactions. However, to establish the effectiveness of such metrics in capturing quantum chaotic features, it is crucial to demonstrate their ability to detect state sensitivity in more realistic systems, particularly those already known to exhibit quantum chaos based on other criteria.

In this study, we investigate the dynamics of a quantum kicked top system consisting of  $n$  qubits [18,36], with an interaction energy parametrized as  $\alpha$ . We examine how a small initial perturbation evolves over time in this system. It is well established that as the value of  $\alpha$  increases, the system undergoes a quantum order-to-chaos transition [2,39]. To quantify the effect of perturbations, we use QHD. Our analysis reveals that QHD effectively detects hypersensitivity to perturbations for  $\alpha > 3$ . This result establishes a meaningful connection between classical and quantum chaotic behaviors, shedding light on the intuitive links between the two.

### III. KICKED TOP

The classical kicked top model describes the dynamics of an angular momentum vector  $\mathbf{J}$ , which is governed by the Hamiltonian  $H(t) = H_0 + H_1 \sum_{n=-\infty}^{+\infty} T \delta(t - nT)$ . Here,  $H_0 = \beta J_y$  represents the natural dynamics, and  $H_1 = \frac{\alpha}{2J} J_z^2$  represents the “kicks” that occur periodically with a period of  $T$ . It is well established that the model undergoes a transition from order to chaos as the parameter  $\alpha$  increases. This transition generally takes place in the regime  $1 < \alpha < 6$ .

Here, we examine the quantum version of the kicked top model implemented on spin  $s = n/2$ , which is equivalent to a system of  $n$  interacting qubits. The dynamics is discrete, and a single step of the evolution can be described by the following equation,

$$|\psi_{t+1}\rangle = U_1 U_2 |\psi_t\rangle, \quad (14)$$

where

$$U_1 = e^{i\frac{\alpha}{4n} \sum_{i,j=1}^n \sigma_z^{(i)} \sigma_z^{(j)}}, \quad (15)$$

and

$$U_2 = e^{i\frac{\beta}{2} \sum_{i=1}^n \sigma_y^{(i)}}. \quad (16)$$

In the above equation,  $\sigma_j^{(i)}$  represents the Pauli- $j$  matrix (where  $j = x, y, z$ ) acting on the  $i$ th qubit. In physical terms, this model describes a system of spin-1/2 particles in a magnetic field with a magnitude proportional to  $\beta$ . The spins naturally precess, but their motion is periodically interrupted

by pairwise interactions. The energy of interaction is proportional to  $\alpha$ . To simplify the equations of motion, it is common to choose  $\beta = \pi/2$ . However, even with this choice, the system can exhibit intricate behaviors. Notably, it has been demonstrated in Ref. [28] that a quantum analog of the order-to-chaos transition can be observed within the same range of  $\alpha$ .

#### IV. METHODS

We conduct a numerical investigation into the evolution of the aforementioned system for  $\beta = \pi/2$ , exploring various choices of  $\alpha$ . In each simulation run, we initialize the system in the symmetric pure product state  $\rho_0 = |\psi_0\rangle\langle\psi_0|$ , where  $|\psi_0\rangle = |\chi\rangle^{\otimes n}$ , with  $|\chi\rangle = \cos\theta|0\rangle + e^{i\phi}\sin\theta|1\rangle$ . The parameters  $\theta$  and  $\phi$  are randomly chosen. These symmetric qubit states, known as coherent spin states [48], are considered the most classical spin states as they minimize the uncertainty of the spin- $n/2$  operators  $S_j = \frac{1}{2}\sum_{i=1}^n\sigma_j^{(i)}$ . The coherent spin states are eigenstates of the spin operator  $S_{\mathbf{k}}|\psi_0\rangle = \frac{n}{2}|\psi_0\rangle$ , where  $\mathbf{k} = (\cos\phi\sin\theta, \sin\phi\sin\theta, \cos\theta)$  represents the axis onto which the spin- $n/2$  is projected,  $S_{\mathbf{k}} = \mathbf{k} \cdot \mathbf{S}$ , and  $\mathbf{S} = (S_x, S_y, S_z)$ .

Furthermore, we examine the evolution of the perturbed (pure) state  $\rho'_0 = |\psi'_0\rangle\langle\psi'_0|$ , where  $|\psi'_0\rangle = |\chi'\rangle^{\otimes n}$ .  $|\chi'\rangle$  is given by  $|\chi'\rangle = R_\varphi|\chi\rangle$ , where  $R_\varphi = e^{i\frac{\varphi}{2}\sigma_{\mathbf{m}}}$  denotes a single-qubit rotation about a randomly chosen  $\mathbf{m}$  axis,  $\sigma_{\mathbf{m}} = \mathbf{m} \cdot \mathbf{s}$  and  $\mathbf{s} = (\sigma_x, \sigma_y, \sigma_z)$ . The rotation angle is denoted by  $\varphi$  ( $\varphi \ll 1$ ). Finally, we evaluate the distance  $D(\rho_t, \rho'_t)$  and analyze its dependence on the parameters  $t$ ,  $\varphi$ , and  $\alpha$ .

It is important to note that both the initial state  $\rho_0$  and the perturbed state  $\rho'_0$  are symmetric, meaning they remain unchanged under the permutation of spins. This symmetry is preserved throughout the evolution due to the symmetric nature of the evolution operators  $U_1$  and  $U_2$ . Consequently, the states  $\rho_t$  and  $\rho'_t$  also maintain their symmetry. As a result, the dynamics of the  $n$ -qubit system occur within a symmetric subspace of dimension  $n+1$ . This characteristic significantly simplifies the complexity of numerical simulations and facilitates the analysis of the obtained data.

We found that in our numerical simulations, the optimal partition is a partition of the system into single qubits, i.e.,  $a_{\max} = n, k_a = 1$  for each  $a$ . Because the system is symmetric, we get

$$D(\rho_t, \rho'_t) = \frac{n}{2} \text{Tr}|\tilde{\rho}_t - \tilde{\rho}'_t|, \quad (17)$$

where  $\tilde{\rho}_t$  is the state of a single-qubit subsystem of  $\rho_t$  and  $\tilde{\rho}'_t$  is the state of a single-qubit subsystem of  $\rho'_t$ . The general method of how to evaluate states of subsystems is given in Appendix B.

Finally, the value of  $D(\rho_t, \rho'_t)$  differs from one simulation to the other because it depends on the initial state that is chosen randomly. That is why we introduce average distance

$$\mathcal{D}_t = \langle D(\rho_t, \rho'_t) \rangle_{\rho_0}, \quad (18)$$

in which we average over 100 numerical runs. Therefore,  $\mathcal{D}_t$  reflects a property of the system, not a property of a particular

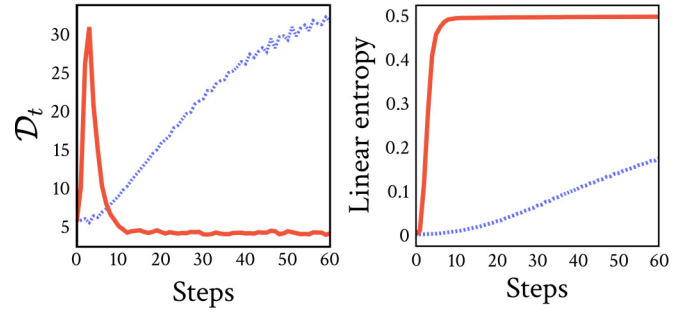


FIG. 1. Left: The plot of  $\mathcal{D}_t$  for  $n = 1000$  and  $\varphi = 0.01$ . The points were joined for better visibility. The red (solid) plot corresponds to  $\alpha = 6$  and the blue (dotted) one to  $\alpha = 1$ . Right: The corresponding growth of the single-qubit entropy.

state. Note also that for  $\varphi \ll 1$  the initial distance

$$D(\rho_0, \rho'_0) = \frac{n\varphi}{2} \quad (19)$$

is independent of the initial state (see Appendix C).

#### V. RESULTS

Our most important finding is that  $\mathcal{D}_t$  can be used as a witness of quantum chaos. In particular, it grows rapidly for the values of  $\alpha$  corresponding to the chaotic regime and slowly for the values corresponding to the regular regime. An example of such behavior is presented in Fig. 1 (left), where we consider the system of  $n = 1000$  qubits and the perturbation angle  $\varphi = 0.01$ . We compare two cases,  $\alpha = 6$  (red plot) and  $\alpha = 1$  (blue plot).

Interestingly, in the chaotic regime  $\mathcal{D}_t$  grows fast and then it decreases fast, resulting in a peak. The reason for this behavior comes from the fact that  $\mathcal{D}_t$  is an averaged comparison between single-qubit substates  $\tilde{\rho}_t$  and  $\tilde{\rho}'_t$ . They initially diverge ( $\mathcal{D}_t$  grows), but due to the entangling nature of the kicked top dynamics they get more entangled with the rest of the system, therefore they become more mixed. The more mixed they become, the more similar they get ( $\mathcal{D}_t$  decreases).

The amount of entanglement between the qubit and the rest of the system can be measured by linear entropy  $S_t = 1 - \text{Tr}(\tilde{\rho}_t^2)$ . An example of how  $S_t$  changes in time is represented in Fig. 1 (right). It is clear that the peak in  $\mathcal{D}_t$  matches the growth of  $S_t$ . Note that the fast growth of entanglement within the multipartite system is usually considered to be a signature of quantum chaos [18–20,32,36,37,40,49,50] (for a detailed discussion, see Ref. [41]). The entanglement time is analogous to the Ehrenfest time  $t_E$ , the time after which the correspondence principle is no longer valid. Intuitively, this happens when the uncertainties are of the order of the size of the system, which is exactly what is manifested by entangled states.

Because of the above, the position of the peak of  $\mathcal{D}_t$  can be considered as the Ehrenfest time of the system. In Fig. 2 we show how  $\mathcal{D}_t$  depends on the number of qubits  $n$ . It is expected [20,51,52] that Ehrenfest time scales as  $t_E \sim h_{\text{eff}}^{-1/2}$  for regular and as  $t_E \sim \ln(h_{\text{eff}}^{-1})$  for chaotic dynamics, where  $h_{\text{eff}}$  is the effective Planck constant. For systems confined to the

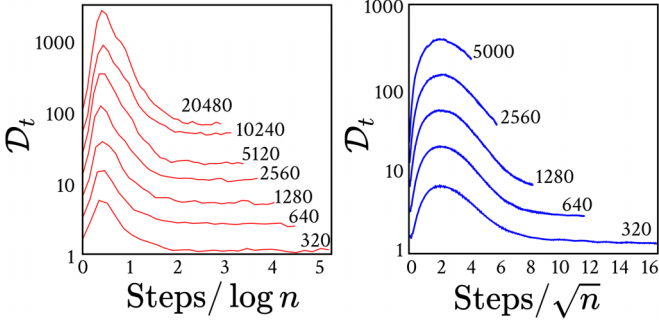


FIG. 2. The plots of  $\mathcal{D}_t$  for  $\varphi = 0.01$  and different values of  $n$ . It is visible that the Ehrenfest time scales as  $\ln n$  for  $\alpha = 6$  and as  $\sqrt{n}$  for  $\alpha = 1$ .

symmetric subspace the effective Planck constant is [20,53] inversely proportional to the dimension of this subspace. Thus we expect  $t_E \sim n^{1/2}$  for regular and as  $t_E \sim \ln(n)$  for chaotic dynamics. The position of the peaks in Fig. 2 roughly fulfills this expectation. This confirms that our quantum chaos witness based on  $\mathcal{D}_t$  is in accordance with the usually used ones.

Another interesting problem is to investigate if our quantum chaos witness works in the range for which both chaotic and regular behaviors are known to coexist ( $1 < \alpha < 6$ ). In this case, the chaotic properties of the system depend on the initial state and we can no longer use the averaged witness  $\mathcal{D}_t$ . Instead, we return to  $D(\rho_t, \rho'_t)$ . Moreover, we relate the observed quantum behavior to the behavior of classical trajectories with analogous initial conditions. The method for evaluating classical trajectories is given in Appendix D.

In Fig. 3 we show two examples for  $\alpha = 2.3$ . In the first one (blue, dotted) the initial conditions  $\theta$  and  $\phi$  correspond to a classical regular trajectory (see Fig. 3, right). It is clear that in this case  $D(\rho_t, \rho'_t)$  does not change much (see Fig. 3, left). The second example (red, solid) corresponds to a classical chaotic trajectory and it is well visible that in this case  $D(\rho_t, \rho'_t)$  grows. This observation confirms that our approach could be also used to witness quantum chaos in the transition region.

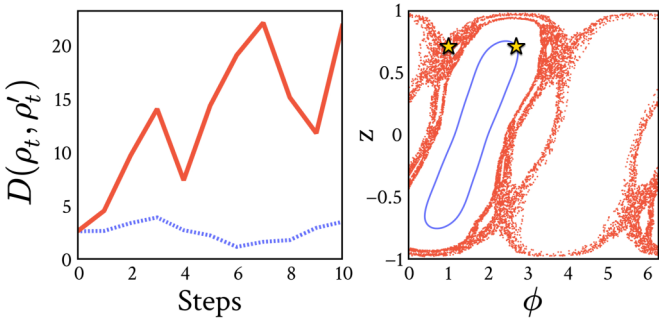


FIG. 3. Left: The plot of  $D(\rho_t, \rho'_t)$  for  $n = 500$ ,  $\varphi = 0.01$ , and  $\alpha = 2.3$ . This value of  $\alpha$  corresponds to both chaotic and regular behaviors. The evolution depends on the choice of initial conditions determined by  $\theta$  and  $\phi$  [red (solid) and blue (dotted)]. Right: The corresponding classical trajectories for the analogous initial conditions. Stars mark starting points.

VI. CONCLUSIONS

We demonstrated that in the case of quantum systems one can detect chaos using a quantum Hamming distance [27] (QHD) in Hilbert space. We analyzed the quantum kicked top dynamics of  $n$  qubits and found that QHD between two quantum states can rapidly grow. This finding confirms the results of Ref. [22], namely that just as classical chaotic dynamics, quantum chaotic dynamics is hypersensitive to perturbations.

Our method of detecting quantum chaos is in accordance with previously developed methods. For example, we found that the growth of QHD matches the growth of entanglement [41]. Moreover, we argued that the time after which QHD reaches its maximum corresponds to the Ehrenfest time  $t_E$  [20,51,52], which scales as  $n^{1/2}$  and  $\log(n)$  in the regular and chaotic regimes, respectively. Finally, we showed that QHD can be used to distinguish between regular and chaotic dynamics in situations where the system exhibits both behaviors for different initial conditions.

In this paper we initiate a research program of studying quantum chaos with the help of QHD. The next step is to investigate other discrete-time systems, continuous-time systems, and continuous-variable systems.

ACKNOWLEDGMENTS

We are grateful to D. Girolami, F. Anzà, and M. Lewenstein for helpful discussions. This research is supported by the Polish National Science Centre (NCN) under the Maestro Grant No. DEC-2019/34/A/ST2/00081. J.W. acknowledges support from IDUB BESTStudentGRANT (No. 010/39/UAM/0010). Part of the numerical studies in this work have been carried out using resources provided by Wrocław Centre for Networking and Supercomputing [54], Grant No. 551 (A.S.S.).

APPENDIX A: ADDITIVITY PROPERTY OF QHD BASED ON TRACE DISTANCE

Here, we prove the additivity of the metric

$$D(\rho, \sigma) = \max_P \delta_P(\rho, \sigma), \tag{A1}$$

where

$$\delta_P(\rho, \sigma) = \sum_a \frac{1}{k_a} d(\rho_a, \sigma_a) \tag{A2}$$

and

$$d(\rho, \sigma) = \frac{1}{2} \text{Tr}|\rho - \sigma|. \tag{A3}$$

The additivity property implies

$$D(\rho_A \otimes \rho_B, \sigma_A \otimes \sigma_B) = D(\rho_A, \sigma_A) + D(\rho_B, \sigma_B). \tag{A4}$$

Assume partition  $P$  into states  $\rho_{AB}^j$  and  $\sigma_{AB}^j$  for which we have  $\delta_P(\rho_{AB}, \sigma_{AB})$ . We will show that we can obtain at least as large  $\delta_{P'}(\rho_{AB}, \sigma_{AB})$  for partition  $P'$ , which is obtained by splitting each  $\rho_{AB}^j$  ( $\sigma_{AB}^j$ ) into  $\rho_A^j$  and  $\rho_B^j$  ( $\sigma_A^j$  and  $\sigma_B^j$ ). We use the following property of trace distance (see Ref. [55]):

$$\begin{aligned} & \frac{1}{2} \text{Tr}|\rho_A \otimes \rho_B - \sigma_A \otimes \sigma_B| \\ & \leq \frac{1}{2} \text{Tr}|\rho_A - \sigma_A| + \frac{1}{2} \text{Tr}|\rho_B - \sigma_B|. \end{aligned} \tag{A5}$$

The above implies

$$\begin{aligned} & \frac{1}{k_A^j + k_B^j} d(\rho_{AB}^j, \sigma_{AB}^j) \\ & \leq \frac{1}{k_A^j} d(\rho_A^j, \sigma_A^j) + \frac{1}{k_B^j} d(\rho_B^j, \sigma_B^j), \end{aligned} \quad (\text{A6})$$

where  $\rho_A^j$  and  $\sigma_A^j$  consist of  $k_A^j$  elementary subsystems and  $\rho_B^j$  and  $\sigma_B^j$  consist of  $k_B^j$  elementary subsystems. Therefore

$$\begin{aligned} & \sum_j \frac{1}{k_A^j + k_B^j} d(\rho_{AB}^j, \sigma_{AB}^j) \\ & \leq \sum_j \frac{1}{k_A^j} d(\rho_A^j, \sigma_A^j) + \sum_j \frac{1}{k_B^j} d(\rho_B^j, \sigma_B^j), \end{aligned} \quad (\text{A7})$$

which implies that maximum is obtained by splitting each  $\rho_{AB}^j$  ( $\sigma_{AB}^j$ ) into  $\rho_A^j$  and  $\rho_B^j$  ( $\sigma_A^j$  and  $\sigma_B^j$ ).

## APPENDIX B: CALCULATION OF $m$ -QUBIT DENSITY MATRIX

As mentioned in the main text, the evolution operators are symmetric. Thus, evolution will be constrained to the  $n+1$ -dimensional effective Hilbert space, provided that the system will be initialized in a symmetric state. This effective Hilbert space is spanned by the Dicke states

$$|d_k^n\rangle = \binom{n}{k}^{-1/2} |n, k\rangle + \text{permutations}. \quad (\text{B1})$$

In the above we use particular states of  $n$  qubits with  $k$  ones and  $n-k$  zeros,

$$|n, k\rangle = |1 \dots 1 0 \dots 0\rangle = |1\rangle^{\otimes k} \otimes |0\rangle^{\otimes n-k}. \quad (\text{B2})$$

Now, let us assume that the  $n$ -qubit system is in the arbitrary symmetric state

$$|\Psi\rangle = \sum_{k=0}^n a_k |d_k^n\rangle, \quad (\text{B3})$$

$$\rho = |\Psi\rangle\langle\Psi| = \sum_{k,k'=0}^n a_k a_{k'}^* |d_k^n\rangle\langle d_{k'}^n|. \quad (\text{B4})$$

We need to consider the subsets of  $m$  qubits achieved via tracing over  $n-m$  qubits. The corresponding  $m$ -qubit subsystem state ( $m \leq n$ ) is given by

$$\rho^{(m)} = \sum_{l=0}^n \langle n-m, l | \rho | n-m, l \rangle + \text{permutations}. \quad (\text{B5})$$

It follows that (for  $l \leq k$ )

$$\begin{aligned} \langle n-m, l | d_k^n \rangle &= \binom{n}{k}^{-1/2} |1\rangle^{\otimes(k-l)} \otimes |0\rangle^{\otimes m-(k-l)} \\ &+ \text{permutations}. \end{aligned} \quad (\text{B6})$$

For  $l > k$  one has  $\langle n-m, l | d_k^n \rangle = 0$ . The same result is obtained for any of  $\binom{n-m}{l}$  permutations of  $|n-m, l\rangle$ . The above

equation (for  $l \leq k$ ) can be also written as

$$\langle n-m, l | d_k^n \rangle = \binom{n}{k}^{-1/2} \binom{m}{k-l}^{1/2} |d_{k-l}^m\rangle. \quad (\text{B7})$$

Therefore

$$\begin{aligned} \rho^{(m)} &= \sum_{k,k'=0}^n a_k a_{k'}^* \binom{n}{k}^{-1/2} \binom{n}{k'}^{-1/2} \\ &\times \sum_l \binom{n-m}{l} \binom{m}{k-l}^{1/2} \binom{m}{k'-l}^{1/2} |d_{k-l}^m\rangle\langle d_{k'-l}^m|. \end{aligned} \quad (\text{B8})$$

Finally, let us define  $p = k-l$  and  $q = k'-l$ . Therefore, the state of  $m$  qubits is given by

$$\begin{aligned} \rho^{(m)} &= \sum_{l=0}^{n-m} \sum_{p,q=0}^m a_{p+l} a_{q+l}^* \binom{n-m}{l} \binom{n}{p+l}^{-1/2} \\ &\times \binom{n}{q+l}^{-1/2} \binom{m}{p}^{1/2} \binom{m}{q}^{1/2} |d_p^m\rangle\langle d_q^m|. \end{aligned} \quad (\text{B9})$$

For  $m=1$  the above formula simplifies to

$$\rho^{(1)} = \tilde{\rho} = \sum_{l=0}^{n-1} \sum_{p,q=0}^1 a_{p+l} a_{q+l}^* M_{pq}(n, l) |p\rangle\langle q|,$$

where

$$M_{00}(n, l) = \frac{1}{n}(n-l),$$

$$M_{01}(n, l) = M_{10}(n, l) = \frac{1}{n} \sqrt{(n-l)(l+1)},$$

and

$$M_{11}(n, l) = \frac{1}{n}(l+1).$$

## APPENDIX C: CALCULATION OF INITIAL DISTANCE

In this Appendix, we prove Eqs. (19) in main text. Without losing generality, let the initial state of a single qubit be

$$\tilde{\rho} = \begin{pmatrix} 1 & 0 \\ 0 & 0 \end{pmatrix}. \quad (\text{C1})$$

The perturbed state is given by

$$\tilde{\rho}' = R_\varphi \tilde{\rho} R_\varphi^\dagger, \quad (\text{C2})$$

where  $R_\varphi = e^{i\frac{\varphi}{2}\mathbf{m}\cdot\mathbf{s}}$  denotes a single-qubit rotation about the  $\mathbf{m}$  axis, with unit vector  $\mathbf{m} = (m_x, m_y, 0)$ , and  $\mathbf{s} = (\sigma_x, \sigma_y, \sigma_z)$ . The rotation angle  $\varphi$  is assumed to be small ( $\varphi \ll 1$ ). The linear in  $\varphi$  approximation gives

$$\tilde{\rho}' = \tilde{\rho} + i\frac{\varphi}{2}[\mathbf{m} \cdot \mathbf{s}, \tilde{\rho}]. \quad (\text{C3})$$

Note that

$$[\mathbf{m} \cdot \mathbf{s}, \tilde{\rho}] = i\mathbf{m}' \cdot \mathbf{s}, \quad (\text{C4})$$

where  $\mathbf{m}' = (m_y, -m_x, 0)$ . Now we have from Eq. (9) in the main text

$$D(\rho, \rho') = \frac{n}{2} \text{Tr}|\tilde{\rho} - \tilde{\rho}'| = \frac{n\varphi}{4} \text{Tr}|\mathbf{m}' \cdot \mathbf{s}| = \frac{n\varphi}{2}. \quad (\text{C5})$$

## APPENDIX D: CLASSICAL KICKED TOP

The dynamics of the classical kicked top is given by the following equation,

$$\begin{pmatrix} x_{t+1} \\ y_{t+1} \\ z_{t+1} \end{pmatrix} = \begin{pmatrix} 0 & \sin(\alpha x_t) & \cos(\alpha x_t) \\ 0 & \cos(\alpha x_t) & -\sin(\alpha x_t) \\ -1 & 0 & 0 \end{pmatrix} \begin{pmatrix} x_t \\ y_t \\ z_t \end{pmatrix}. \quad (\text{D1})$$

The above equation was used to produce the right part of Fig. 3 in the main text. In this figure, we use coordinates  $(\phi, z)$  where  $\phi = \arg(x + iy)$ .

- 
- [1] S. H. Strogatz, *Nonlinear dynamics and chaos: With applications to physics, biology, chemistry, and engineering*, *Studies in Nonlinearity* (CRC Press, Boca Raton, FL, 2000).
- [2] F. Haake, S. Gnutzmann, and M. Kuś, *Quantum Signatures of Chaos*, *Springer Series in Synergetics* (Springer, Berlin, 2018).
- [3] Z. Rudnick, *Not. Am. Math. Soc.* **55**, 32 (2008).
- [4] A. Peres, *Phys. Rev. A* **30**, 1610 (1984).
- [5] A. K. Pattanayak and P. Brumer, *Phys. Rev. Lett.* **77**, 59 (1996).
- [6] A. R. Kolovsky, *Phys. Rev. Lett.* **76**, 340 (1996).
- [7] H. M. Pastawski, P. R. Levstein, and G. Usaj, *Phys. Rev. Lett.* **75**, 4310 (1995).
- [8] T. Gorin, T. Prosen, T. Seligman, and M. Žnidarič, *Phys. Rep.* **435**, 33 (2006).
- [9] S. Pg, V. Madhok, and A. Lakshminarayan, *J. Phys. D: Appl. Phys.* **54**, 274004 (2021).
- [10] B. Yan, L. Cincio, and W. H. Zurek, *Phys. Rev. Lett.* **124**, 160603 (2020).
- [11] B. Swingle, *Nat. Phys.* **14**, 988 (2018).
- [12] I. García-Mata, M. Saraceno, R. A. Jalabert, A. J. Roncaglia, and D. A. Wisniacki, *Phys. Rev. Lett.* **121**, 210601 (2018).
- [13] N. Anand, G. Styliaris, M. Kumari, and P. Zanardi, *Phys. Rev. Res.* **3**, 023214 (2021).
- [14] T. A. Brody, J. Flores, J. B. French, P. A. Mello, A. Pandey, and S. S. M. Wong, *Rev. Mod. Phys.* **53**, 385 (1981).
- [15] L. D’Alessio, Y. Kafri, A. Polkovnikov, and M. Rigol, *Adv. Phys.* **65**, 239 (2016).
- [16] F. Borgonovi, F. Izrailev, L. Santos, and V. Zelevinsky, *Phys. Rep.* **626**, 1 (2016).
- [17] X.-Q. Wang, J. Ma, X.-H. Zhang, and X.-G. Wang, *Chin. Phys. B* **20**, 050510 (2011).
- [18] X. Wang, S. Ghose, B. C. Sanders, and B. C. Hu, *Phys. Rev. E* **70**, 016217 (2004).
- [19] A. Piga, M. Lewenstein, and J. Q. Quach, *Phys. Rev. E* **99**, 032213 (2019).
- [20] A. Leroise and S. Pappalardi, *Phys. Rev. A* **102**, 032404 (2020).
- [21] K. Gietka, J. Chwedeńczuk, T. Wasak, and F. Piazza, *Phys. Rev. B* **99**, 064303 (2019).
- [22] Z. Wang, Y. Wang, and B. Wu, *Phys. Rev. E* **103**, 042209 (2021).
- [23] K. Życzkowski and W. Słomczyński, *J. Phys. A* **31**, 9095 (1998).
- [24] K. Życzkowski and W. Słomczyński, *J. Phys. A* **34**, 6689 (2001).
- [25] S. Friedland, M. Eckstein, S. Cole, and K. Życzkowski, *Phys. Rev. Lett.* **129**, 110402 (2022).
- [26] R. Bistroń, M. Eckstein, and K. Życzkowski, *J. Phys. A: Math. Theor.* **56**, 095301 (2023).
- [27] D. Girolami and F. Anzà, *Phys. Rev. Lett.* **126**, 170502 (2021).
- [28] M. Kuś, R. Scharf, and F. Haake, *Z. Phys. B: Condens. Matter* **66**, 129 (1987).
- [29] M. Kus, J. Mostowski, and F. Haake, *J. Phys. A: Math. Gen.* **21**, L1073 (1988).
- [30] P. Gerwinski, F. Haake, H. Wiedemann, M. Kuś, and K. Życzkowski, *Phys. Rev. Lett.* **74**, 1562 (1995).
- [31] M. Lombardi and A. Matzkin, *Phys. Rev. E* **83**, 016207 (2011).
- [32] S. Ghose and B. C. Sanders, *Phys. Rev. A* **70**, 062315 (2004).
- [33] V. Madhok, C. A. Riofrío, S. Ghose, and I. H. Deutsch, *Phys. Rev. Lett.* **112**, 014102 (2014).
- [34] U. T. Bhosale and M. S. Santhanam, *Phys. Rev. E* **95**, 012216 (2017).
- [35] S. Chaudhury, A. Smith, B. Anderson, S. Ghose, and P. Jessen, *Nature (London)* **461**, 768 (2009).
- [36] C. Neill, P. Roushan, M. Fang, Y. Chen, M. Kolodrubetz, Z. Chen, A. Megrant, R. Barends, B. Campbell, B. Chiaro *et al.*, *Nat. Phys.* **12**, 1037 (2016).
- [37] S. Dogra, V. Madhok, and A. Lakshminarayan, *Phys. Rev. E* **99**, 062217 (2019).
- [38] R. Zarum and S. Sarkar, *Phys. Rev. E* **57**, 5467 (1998).
- [39] F. Haake, M. Kuś, and R. Scharf, *Z. Phys. B: Condens. Matter* **65**, 381 (1987).
- [40] S. Ghose, R. Stock, P. Jessen, R. Lal, and A. Silberfarb, *Phys. Rev. A* **78**, 042318 (2008).
- [41] M. Kumari and S. Ghose, *Phys. Rev. A* **99**, 042311 (2019).
- [42] L. Fiderer and D. Braun, *Nat. Commun.* **9**, 1351 (2018).
- [43] L. Sieberer, T. Olsacher, A. Elben, M. Heyl, P. Hauke, F. Haake, and P. Zoller, *npj Quantum Inf.* **5**, 78 (2019).
- [44] I. Bengtsson and K. Życzkowski, *Geometry of Quantum States* (Cambridge University Press, Cambridge, UK, 2006).
- [45] M. Nielsen and I. Chuang, *Quantum Computation and Quantum Information* (Cambridge University Press, Cambridge, UK, 2010).
- [46] L. Viola, and W. G. Brown, *J. Phys. A: Math. Theor.* **40**, 8109 (2007).
- [47] P. Kurzyński, *Phys. Rev. E* **104**, L052202 (2021).
- [48] M. Kitagawa and M. Ueda, *Phys. Rev. A* **47**, 5138 (1993).
- [49] J. B. Ruebeck, J. Lin, and A. K. Pattanayak, *Phys. Rev. E* **95**, 062222 (2017).
- [50] Y. Weinstein and L. Viola, *Europhys. Lett.* **76**, 746 (2006).
- [51] Z. Chuan and Wu. Biao, *Chin. Phys. Lett.* **38**, 030502 (2021).
- [52] G. Berman, E. Bulgakov, and D. Holm, *Crossover-Time in Quantum Boson and Spin Systems* (Springer, Berlin, 1994).
- [53] B. Sciolla and G. Biroli, *J. Stat. Mech.* (2011) P11003.
- [54] [wcss.pl](http://wcss.pl).
- [55] M. M. Wilde, *Quantum Information Theory* (Cambridge University Press, Cambridge, UK, 2013).